JGR Solid Earth

RESEARCH ARTICLE

10.1029/2020JB020365

Structure and Density of H_2O-Rich Mg_2SiO_4 Melts at High Pressure From Ab Initio Simulations

Liang Yuan[1,2], Gerd Steinle-Neumann[2], and Akio Suzuki[1]

[1]Department of Earth and Planetary Materials Science, Tohoku University, Sendai, Japan, [2]Bayerisches Geoinstitut, Universität Bayreuth, Bayreuth, Germany

Key Points:

- We perform ab initio molecular dynamics simulations on Mg_2SiO_4 melts over a wide range of H_2O concentrations
- We find no evidence for an increase in the degree of melt polymerization with water for ultramafic magmas as proposed previously
- The critical water content at which hydrous peridotitic melts have the same density as the surrounding mantle is about 4 wt%

Supporting Information:

- Supporting Information S1

Correspondence to:
L. Yuan,
liang.yuan@uni-bayreuth.de

Citation:
Yuan, L., Steinle-Neumann, G., & Suzuki, A. (2020). Structure and density of H_2O-rich Mg_2SiO_4 melts at high pressure from ab initio simulations. *Journal of Geophysical Research: Solid Earth*, *125*, e2020JB020365. https://doi.org/10.1029/2020JB020365

Received 7 JUN 2020
Accepted 21 SEP 2020
Accepted article online 23 SEP 2020

Abstract Water has a strong effect on silicate melt properties, yet its dissolution mechanism in depolymerized melts, typical for mantle composition, remains poorly understood. Here we report results of first-principles molecular dynamics simulations for hydrous Mg_2SiO_4 melts with 6, 16, and 27 wt% H_2O at pressure and temperature conditions relevant to the upper mantle and mantle transition zone. The results show that hydrogen bonds not only to the network-forming cation Si but also to Mg which —nevertheless—remains the most important network modifier. There is no evidence to support the hypothesis based on experimental data that water may cause an increase in melt polymerization for ultramafic magmas; the ratio of non-bridging oxygen per Si increases with the addition of the oxygen from H_2O. The partial molar volume of water is independent on concentration in our simulations which allows us to examine the density of hydrous melt systematically. The critical water content—at which melts are neutrally buoyant compared to the surrounding mantle—is ~4 wt% H_2O for a pyrolite composition, much lower than the high water content (>10 wt%) observed in petrological experiments and estimated thermodynamically for low-degree partial melts formed in the vicinity of the mantle transition zone.

Plain Language Summary Geophysical observations indicate abrupt changes in the material properties of the Earth's mantle right below and above the transition zone, at a depth between 410 and 660 km. The existence of low-velocity and high conductivity layers near this region is often taken as an indication for melting caused by the presence of water. However, the density of such hydrous melts is not well characterized over the relevant pressure-temperature range. Here we present new simulations on Mg_2SiO_4 melts with a wide range of water concentrations to address this issue. The water content at which hydrous melts have the same density as the surrounding mantle is about 4 wt%, much lower than the high water content (>10 wt%) estimated for melts occurring in the Earth's mantle, suggesting they cannot experience long-term gravitational stability in the mantle transition zone and its vicinity. We further find that water does not cause a significant change in melt structure as proposed previously.

1. Introduction

Water is thought to play an essential role in the Earth's dynamics, as it fundamentally alters the physical properties of materials in the planet's interior. Geophysical observations have revealed the existence of low-velocity and high conductivity layers above the 410-km (Alex Song et al., 2004; Revenaugh & Sipkin, 1994; Tauzin et al., 2010; Toffelmier & Tyburczy, 2007) and below the 660-km seismic discontinuities (Liu et al., 2016, 2018; Schmandt et al., 2014), presumably indicating the occurrence of hydrous silicate melts. A water-rich mantle transition zone (MTZ) is supported by the observation of ice-VII (H_2O) (Tschauner et al., 2018) and hydrogen within the ringwoodite crystal lattice (Pearson et al., 2014), both found as inclusions in diamonds formed in this depth range. In addition, hydrous minerals such as phase egg ($AlSiO_3OH$) and δ-AlOOH, stable at pressure (P) and temperature (T) conditions of the MTZ, have also been discovered (Wirth et al., 2007). These lines of evidence suggest that the MTZ may contain a substantial amount of water regionally. Alternatively, based on constraints from mineral viscosity, Fei et al. (2017) suggested that the MTZ contains 1–2 wt% water globally.

As water preferentially partitions into melts compared to solid peridotite residues (Aubaud et al., 2004; Novella et al., 2014), partial melts of hydrous material from the MTZ are expected to be water-rich (up to 16.5 wt% H_2O), supported by observations from melting experiments (Freitas et al., 2017; Litasov & Ohtani, 2002; Zhang et al., 2017) and insight from thermodynamic modeling (Hirschmann et al., 2009;

Novella et al., 2017). Whether these water-rich melts stay at depth—and therefore provide a viable explanation for the geophysical observations—is an open question, as they appear to be far too water-rich to be neutrally buoyant. However, iron also becomes enriched in partial peridotite melts (Kawamoto & Holloway, 1997; Zhang & Herzberg, 1994), which increases melt density (ρ) substantially. Experiments determining ρ suggest that melts with up to 6–7 wt% H_2O may be gravitationally stable at the 410-km seismic discontinuity (Matsukage et al., 2005; Sakamaki et al., 2006). On the other hand, magmas contributing to the formation of large igneous provinces (LIPs)—though they contain less water (~2 wt% H_2O) (Kuritani et al., 2019)—are still buoyant enough to propagate to the surface from near-MTZ storage (Tian et al., 2016; Zhao et al., 2009).

Hydrogen incorporation in silicate melts has been generally understood in terms of the reaction:

$$H_2O + \text{Si-O-Si} \rightarrow 2\text{Si-OH}. \quad (1)$$

The water molecule breaks up the network structure by converting one bridging oxygen, Si-O-Si, to two non-bridging oxygen (Stolper, 1982). Computations on the SiO_2-H_2O systems over a wide range of H_2O contents (4–23 wt% H_2O) (Karki & Stixrude, 2010; Pöhlmann et al., 2004; Spiekermann et al., 2016) have provided valuable insight into melt structure and dynamics and confirmed that water dissolution mechanism in polymerized melts mainly involves dissociation of H_2O following Reaction 1.

The addition of water to depolymerized melts, on the other hand, has been proposed to potentially result in an increase of polymerization (Mysen & Cody, 2005; Xue & Kanzaki, 2004). In particular, structure factors determined by in situ X-ray diffraction on water-rich silicate melts with 15–20 wt% H_2O support this hypothesis due to the interaction between water species and Mg cations indicated by the reaction (Yamada et al., 2007, 2011):

$$\text{Si-O-Mg} + \text{Si-O-H} \rightarrow \text{Si-O-Si} + \text{Mg-O-H}. \quad (2)$$

In carbonated silicate melts, Moussallam et al. (2016) found that CO_3^{2-}-ions can alter the role of Ca and Mg cations from their usual depolymerizing role in breaking up the covalent silicate network, causing a significant polymerization of the melt.

Solid evidence of the polymerization effect of H_2O dissolution on the network structure, however, has been lacking. To quantify the degree of melt polymerization, one needs to know the abundance of bridging oxygen. This is usually approached from experiments by deconvoluting ^{29}Si nuclear magnetic resonance (NMR) or Raman spectra as outlined, for example, by Moussallam et al. (2016), which may result in ambiguities in band assignment and non-unique solution, however. A detailed analysis of the local atomic structure is required, which is currently beyond the reach of experimental studies based on total X-ray and neutron structure factors or NMR and Raman spectroscopy. The structure of water-rich silicate melts and hydrogen speciation further remain elusive in part because these melts are difficult to quench to glass, or it is difficult to account for H_2O lost during *T*-quench (Agee, 2008; Gavrilenko et al., 2019; Hirschmann et al., 2009; Mysen & Cody, 2005; Mysen & Wheeler, 2000).

Considerable experimental efforts have been made to investigate the role of water in controlling silicate melt properties, for example, density (Matsukage et al., 2005; Mookherjee et al., 2008; Ochs & Lange, 1999; Sakamaki et al., 2006), viscosity (Dingwell et al., 1996; Fei et al., 2017; Poe et al., 2006; Richet et al., 2000), diffusivity, and electrical conductivity (Gaillard, 2004; Ni et al., 2011; Pommier et al., 2008). Experiments have been supplemented by molecular dynamics (MD) simulations based on density functional theory (DFT) that investigate the high-*P* dissolution and incorporation behavior of H_2O (Bajgain et al., 2015; Karki & Stixrude, 2010; Mookherjee et al., 2008; Pöhlmann et al., 2004; Spiekermann et al., 2016) and CO_2 (Ghosh et al., 2017; Ghosh & Karki, 2017; Moussallam et al., 2016) in silicate melts. They provide complementary information to experiments, as the DFT-MD approach gives insight into the structure of melts at an atomic scale and allows access to conditions that are not readily explored by experiments. While DFT-MD simulations on the silica-H_2O system (Spiekermann et al., 2016) did explore water-rich compositions (23 wt% H_2O), the vast majority of previous theoretical investigations have focused on probing the behavior of silicate-H_2O systems containing hydrogen with water contents typically not exceeding 10 wt

% (e.g., Bajgain et al., 2015; Karki & Stixrude, 2010; Mookherjee et al., 2008). Here we go beyond this H_2O content, following the suggestions of high water concentrations in silicate melts formed near the MTZ (Freitas et al., 2017; Hirschmann et al., 2009; Novella et al., 2017), and perform DFT-MD simulations on hydrous forsterite (Mg_2SiO_4) melts with 16.6 wt% and 26.7 wt% H_2O and compare the results to those of a more typical composition considered in simulations with 5.5 wt% H_2O. With these simulations, we explore whether H_2O has a polymerizing effect on depolymerized silicate melts as proposed by previous experiments (Mysen & Cody, 2005; Xue & Kanzaki, 2004; Yamada et al., 2007, 2011), and we constrain the influence of H_2O on melt densities—and therefore buoyancy—in the MTZ and its vicinity.

2. Computational Details

We conduct first-principles electronic structure calculations based on Kohn-Sham (KS) DFT to obtain total energy, Hellmann-Feynman stresses (diagonal terms only) and forces with a plane wave approach and periodic boundary conditions using the Vienna ab initio simulation package (Kresse & Furthmüller, 1996; Kresse & Hafner, 1993) and a planewave energy cutoff of 450 eV which is sufficient to obtain converged results for both energy and pressure. We use the projector augmented wave implementation and atomic files (Kresse & Joubert, 1999) and the generalized gradient approximation to exchange and correlation (Perdew et al., 1996). Electronic KS-DFT states are calculated at the Brillouin zone center only.

Molecular dynamics simulations are performed in the canonical *N-V-T* ensemble, where the number of atoms (N) and the volume (V) of the cell is held fixed, and T is controlled by a Nosé-Hoover thermostat (Hoover, 1985). After convergence of the electronic cycle, atoms are advanced with a time step (Δt) of 0.25 fs due to the presence of hydrogen in the system. Run durations are varied from 10 to 20 ps. We double the weight of hydrogen to that of deuterium, following the approach of Pan and Galli (2016) and Schwegler et al. (2008), as this permits the integration of the equations of nuclear motion with larger time steps. We find that assigning deuterium mass to hydrogen affects H dynamics (section 3.5) but has no influence on other transport or structural properties in the liquid (supporting information Figure S1). However, we calculate the density of the melts using the atomic mass of hydrogen. Initial melting and equilibration are performed at 8,000 K and followed by quenching to the desired T of 1,800 and 2,200 K at constant volume. During structure analysis, the configurations until equilibration (initial 2.5 ps) were discarded to ensure no correlation with the structure at 8,000 K. A volume range of $V = 1.2V_X$ to $0.7V_X$ (with $V_X = 1{,}033.5$ Å^3) for the simulation cells is generated to cover P relevant for the upper mantle and the MTZ between 0 and 15 GPa (Table S1). Empirical corrections (e.g., Mookherjee et al., 2008; Stixrude & Karki, 2005) to the resulting P computed by Hellmann-Feynman stresses are not applied.

We set up H_2O-bearing forsterite (Mg_2SiO_4) liquids in cubic supercells with compositions of $22Mg_2SiO_4 + 10H_2O$ (184 atoms), $18Mg_2SiO_4 + 28H_2O$ (210 atoms) and $13Mg_2SiO_4 + 37H_2O$ (202 atoms), corresponding to water contents of 5.5, 16.6, and 26.7 wt% ("fo06H_2O," "fo17H_2O," and "fo27H_2O"), respectively (Table 1). To compare the compressibility of water in silicate melt to that of pure water, additional simulations on a supercell containing 70 H_2O molecules are performed. As Mg_2SiO_4 forsterite—with a melting point of 2,163 K at ambient P and an initial melting slope of 314 K/GPa (Ohtani & Kumazawa, 1981)—is not stable under many of the conditions considered in this study, we cannot compute a dry reference by DFT-MD directly. To compare to dry forsterite liquid, we use the thermodynamic description of de Koker et al. (2008) for Mg_2SiO_4 liquid and extrapolate it to the metastable low-T region.

The high H_2O-content in our simulations raises the question on whether demixing occurs. An inspection of the equilibrated liquid structure and radial distribution functions (RDF) $g(r)$ shows a homogeneous phase even for fo27H_2O. This observation is supported by two experimental inferences: (i) Novella et al. (2017) suggested that Mg_2SiO_4 + 20.4 wt% H_2O is a single liquid phase at high P and T based on quench textures of their samples; (ii) phase relations of the peridotite-H_2O system (22–63 wt% H_2O) studied by in situ X-ray radiography (Mibe et al., 2007) indicate that at $P > 4$ GPa the miscibility gap between silicate melt and fluid is closed; that is, hydrous silicate melt and aqueous fluid in the deep upper mantle become indistinguishable from each other. However, our observation of a homogeneous phase is not sufficient to claim that fo27H_2O is thermodynamically stable: Phase separation rarely occurs spontaneously in regular DFT-MD simulations, a problem that partly arises from the fact that an interface between two phases is not stable in small systems

Table 1
Parameters of the Equation of State Obtained by the Birch-Murnaghan Fit for Mg_2SiO_4 and H_2O

Name	Atoms in supercell	ρ_0 (g/cm^3)	K_0 (GPa)	K'	a	b	c	d
Mg_2SiO_4	$16Mg_2SiO_4$[a]	2.58	33.71	4.00[b]	5.94	−13.40	11.08	−3.21
fo06H_2O	$22Mg_2SiO_4 + 10H_2O$	2.52	37.22	4.00[b]	5.75	−11.65	9.22	−2.62
fo17H_2O	$18Mg_2SiO_4 + 28H_2O$	2.22	28.34	4.00[b]	32.01	−91.99	91.75	−31.46
fo27H_2O	$13Mg_2SiO_4 + 37H_2O$	2.00	23.81	4.00[b]	10.52	−26.58	26.59	−9.63
H_2O (in silicate melt)		1.16	13.34	3.62	16.09	−38.87	35.39	−11.51
H_2O (pure)	$70H_2O$	0.98	4.68	5.27	30.60	−113.41	143.81	−62.00

[a]From de Koker et al. (2008); we extrapolated their high-T results to 1,800 K for pressures between 0 and 16 GPa and fit a second-order Birch-Murnaghan equation of state. a, b, c, and d are parameters for the thermal pressure $B_{TH}(V) = [a + bu + cu^2 + du^3]/1{,}000$ (in units of GPa/K), where $u = V/V_0 = \rho_0/\rho$. [b]Fixed for the fitting of second-order Birch-Murnaghan equation of state.

(Hong & Van De Walle, 2013). For a quantitative evaluation of phase stability, it is necessary to compute the Gibbs energy of solvation of liquid H_2O in Mg_2SiO_4 melts by using thermodynamic integration (e.g., Yuan & Steinle-Neumann, 2020), for example. However, this approach is prohibitively expensive for the problem at hand and beyond the scope of this study.

Our simulated T-range is close to the melting point of the H_2O-bearing system (e.g., Novella et al., 2017), permitting direct comparison to experiments, and considerably lower than previous DFT-MD simulations on hydrous silicate melts (Bajgain et al., 2015; Karki & Stixrude, 2010; Mookherjee et al., 2008; Stixrude & Karki, 2005). Simulations at such low T may not readily reach equilibrium, but we find in our results that they are relevant for liquid properties. We check that the cells considered are indeed in the molten state by monitoring the mean-square displacement (MSD) of all species and $g(r)$ between them. The MSD-t curve displays three regimes (Figure S2): (i) at short times $t < 0.1$ ps, ballistic and vibrational motion of atoms around their local equilibrium dominate, (ii) followed by a range where the atoms are temporarily confined in a cage made of their nearest neighbors, (iii) in the t range of >1 ps, the atoms leave their cages and display a typical diffusional displacement, following the linear Einstein relationship. For fo06H_2O at 1,800 K, we have looked beyond these indicators and performed additional simulations and analysis to support this notion:

1. By performing a series of simulations from 1,600 to 3,600 K at comparable P (Figure S3a), we find that the calculated self-diffusion coefficients of all species closely follow an Arrhenian relation. This behavior suggests that the liquid-glass transition does not occur over this T-range, as diffusion is expected to deviate from an Arrhenian relationship near the glass transition temperature (Hui & Zhang, 2007; Karki et al., 2013).
2. Extending the simulation duration to 100 ps, we find no significant changes in terms of liquid structure and transport properties (Figure S3b).

3. Results and Discussion

3.1. Equation of State

We describe the P-V-T results obtained for fo06H_2O, fo17H_2O, fo27H_2O, and H_2O by combining an isothermal (T_0 = 1,800 K) Birch-Murnaghan equation of state (P_{iso}) of second order (third order for H_2O) with the Mie-Grüneisen model for the thermal contribution (B_{TH}) to P (Bajgain et al., 2015):

$$P(V, T) = P_{iso}(V, T_0) + B_{TH}(V)(T - T_0). \quad (3)$$

The thermal P coefficient $B_{TH}(V)$ is described by

$$B_{TH}(V) = \left[a + bu + cu^2 + du^3\right]/1{,}000, \quad (4)$$

where a, b, c, and d are constants and $u = V/V_0 = \rho_0/\rho$, with V_0 (ρ_0) the zero pressure/equilibrium volume (density) at 1,800 K. Fit parameters are summarized in Table 1; results and fits are displayed

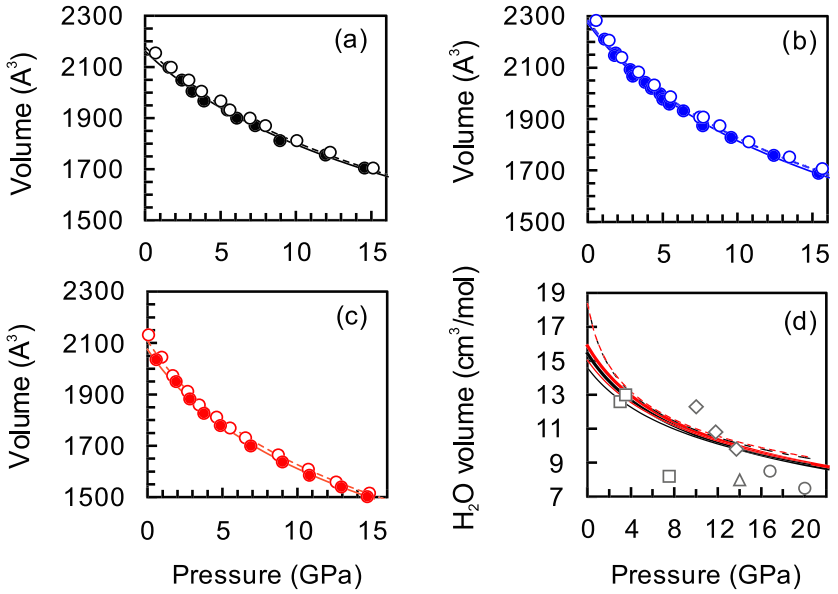

Figure 1. Calculated pressure-volume relations for (a) fo06H_2O (5.5 wt% H_2O), (b) fo17H_2O (16.6 wt% H_2O), and (c) fo27H_2O (26.7 wt% H_2O). Results at 1,800 K (solid symbols) and 2,200 K (open symbols) are fitted using a second-order Birch-Murnaghan equation of state (solid: 1,800 K; dashed: 2,200 K). (d) Partial molar volume of water in silicate melts (solid lines) and molar volume of pure water (dashed lines) at 1,800 K (black) and 2,200 K (red). Thick solid lines represent the mean volume ($\overline{V}_{H_2O}$) of H_2O calculated from the V differences between fo06H_2O, fo17H_2O, and fo27H_2O. Thin solid lines represent $\overline{V}_{H_2O}$ calculated using the dry Mg_2SiO_4 melt (de Koker et al., 2008) as a reference. Also shown are experimental data from the literature for mafic/ultramafic silicate melts: Agee (2008) (squares); Jing and Karato (2012) (diamonds); Matsukage et al. (2005) (triangles); Sakamaki et al. (2006) (circles).

in Figures 1a–1c. Thermal P increases systematically with compression, consistent with previous work on dry and hydrous $MgSiO_3$ melts (Mookherjee et al., 2008; Stixrude & Karki, 2005).

The equation of state fit for the various hydrous Mg_2SiO_4 melts (Table 1) allows us to calculate the partial molar volume of H_2O in the silicate melts (Figure 1d). Differences between fo06H_2O, fo17H_2O, and fo27H_2O at 1,800 K yield molar volume of water in silicate melt ($\overline{V}_{H_2O}$) that are within 3% of one another for the various possible combinations; that is, $\overline{V}_{H_2O}$ does not depend on H_2O concentration in the melt, and we display an average value in Figure 1d. These $\overline{V}_{H_2O}$ differ from those calculated using the volume difference between hydrous Mg_2SiO_4 liquids (this study) and extrapolated dry Mg_2SiO_4 melt (de Koker et al., 2008) by ~5% at ambient P and <1% at $P > 10$ GPa. Higher $T = 2{,}200$ K results in insignificantly larger values for $\overline{V}_{H_2O}$. Values for $\overline{V}_{H_2O}$ decrease from ~15 cm^3/mol at ambient P to ~10 cm^3/mol at 13.4 GPa. At low P, $\overline{V}_{H_2O}$ is significantly smaller than that computed for molecular H_2O (V_{H_2O}), but pure H_2O is initially more compressible than H_2O dissolved in the silicate melt. Therefore, for $P > 4$ GPa, $V_{H_2O} > \overline{V}_{H_2O}$, but both show a similar P-dependence (Figure 1d). Experimental measurements of $\overline{V}_{H_2O}$ show a large variation, and our calculated values for $\overline{V}_{H_2O}$ compare favorably with data at 3–4 GPa by Agee (2008) and at 12–14 GPa by Jing and Karato (2012), but are higher by ~20% than the values by Matsukage et al. (2005) and Sakamaki et al. (2006) in hydrous mafic/ultramafic magmas. A plausible explanation for this discrepancy is that these experiments suffered from water loss at high P and T, an aspect that was examined by Agee (2008) who found that after 30 s at $T = 2{,}023$–$2{,}133$ K the experimental charge retained only 2 wt% H_2O of the 5 wt% in the starting material. Matsukage et al. (2005) and Sakamaki et al. (2006) did not report the H_2O content of their recovered samples as they found their samples to consist of dendritic quenched crystals, interstitial glasses, and pores, which makes any compositional analysis challenging.

Our predicted ambient-P density $\rho_0 = 2.52$ g/cm^3 for fo06H_2O (5.6 wt% H_2O) is comparable to that of a multicomponent realistic melt analog to MORB (4.9 wt% H_2O, iron-free) simulated previously (Bajgain et al., 2015), despite the difference in composition. H_2O leads to a ρ-decrease in the melt by $\Delta\rho = 22$–27 mg/cm^3 per 1 wt

% H_2O at 1,800 K in the *P*-range of 0–15 GPa, in good agreement with experimental data (Matsukage et al., 2005), despite the difference in absolute values for $\overline{V}_{H_2O}$ mentioned. The calculated $\Delta\rho$ due to H_2O dissolution is slightly larger than that induced by CO_2 with $\Delta\rho$ ~ 15 mg/cm^3 per 1 wt% CO_2 (Ghosh et al., 2017).

3.2. Hydrogen Speciation

The speciation of hydrogen in silicate melts can be characterized in terms of coordination environments of hydrogen by oxygen (HO_n); the coordination environments of oxygen by hydrogen (OH_n) provides complementary information. The O-H RDF is governed by a narrow maximum at a distance of ~1.0 Å, followed by a first minimum. The position of this minimum (r_{min}) is frequently used for local atomic structure analysis, in this case to obtain HO_n and OH_n. With increasing *P*, r_{min}, however, becomes poorly defined. The abundance of HO_n in the hydrous silicate systems (and also OH_n in the pure water system) strongly depends on the cutoff value which determines the distance between O and H atoms for the first coordination sphere of atoms that are directly bonded to the reference atom (Figure S4). A small proportion of the hydrogen atoms are not bonded to oxygen when r_{min} values are used for the analysis of H-speciation which is physically and chemically unreasonable. Starting from the position of the first sharp peak, we slowly increase the cutoff distance until all H atoms are bound to the O atoms; that is, the proportion of HO_0 reduces to zero, determining a critical value (r_c). The r_c values show little or no dependence on *P* (Figure S5). Average r_c values determined for the pure H_2O system at 1,800 K (r_c = 1.41 Å) and 2,200 K (r_c = 1.48 Å) are therefore used to examine hydrogen-oxygen coordination (HO_n and OH_n).

An inspection of the partial RDFs reveals that H atoms exclusively form bonds with the only anion in the melt, that is, the O atom. We observe a peak in the RDF for H-H at ~0.7 Å in a few simulations (Figure S6 and Table S1) for the fo17H_2O composition, which suggests the presence of metastable H_2 molecules. The simulation results show that hydrogen in the silicate melts typically occurs as OH_1 hydroxyl groups, OH_2 water molecule, and bridging HO_2 (-O-H-O-**)**. The abundances of HO_n speciation in the hydrous silicates with 5.5, 16.6, and 26.7 wt% H_2O are very similar for a given *P* and *T* (Figure 2). The speciation of hydrogen is sensitive to variations in *P* and shows a weak dependence on *T*. Between 0 and 15 GPa, the proportion of hydroxyl groups (HO_1) in the three hydrous silicate systems gradually decreases from 0.95 to 0.85 at 1,800 K (Figures 2a, 2e, and 2i) and from 0.90 to 0.80 at 2,200 K (Figures 2b, 2f, and 2j). Concurrently, the proportion of bridging -O-H-O- (HO_2) gradually increases with *P*, reaching 0.15 at 1,800 K and 0.20 at 2,200 K. Our results are consistent with observations from prior DFT-MD simulations on $MgSiO_3$-H_2O systems that show a changing role of hydrogen from network modifier to network former (Karki & Stixrude, 2010; Mookherjee et al., 2008).

In the water-poor fo06H_2O liquid, the abundance of molecular water OH_2 is negligible over the whole *P*-range considered (Figure 2), and more than 80% of O atoms do not bond to H at all (OH_0). With increasing bulk water content and increasing O/cation (especially O/Si) ratio, both OH_1 and OH_2 complexes increase in abundance. The total proportion of H-bonded oxygen (OH_1 and OH_2) becomes comparable to that of unbound oxygen (OH_0) as the water content increases to 17 wt%. At ambient *P*, for fo27H_2O, OH_1 is most abundant (>0.4) and unbound oxygen (~0.3) still outnumber OH_2 molecules (~0.2). With compression, the proportion of OH_1 groups stays constant, and OH_2 groups become slightly more abundant at the expenses of the OH_0 group—their abundances are comparable at the highest *P* explored in this study.

3.3. Oxygen Coordination Environment and Polymerization

Oxygen is the most abundant element in silicate melts, where it occurs as "bridging" (BO), "non-bridging" (NBO), and as "free oxygen." BOs link two SiO_n polyhedra (n = 4 and 5 for the *P*-range considered in this study), providing strong bonds between the smallest structural units of the silicate network (left-hand side of Reaction 1 and right-hand side of Reaction 2). The degree of polymerization of a silicate composition is often parameterized by (i) the number of NBO per Si cation, NBO/Si, that can vary from 0 (*fully polymerized*) to 4 (*fully depolymerized*) (Mysen & Richet, 2005) and (ii) the mole fraction of NBO (x_{NBO}, the number of NBO per oxygen) (e.g., Lee et al., 2020); NBO/Si and x_{NBO} are critical in determining the thermodynamic and dynamic properties of melts (Mysen & Richet, 2005; Ni et al., 2015). In our analysis, we count an O atom with two or more Si atoms as nearest neighbors as BO, an O atom with one Si atom as the nearest neighbor as

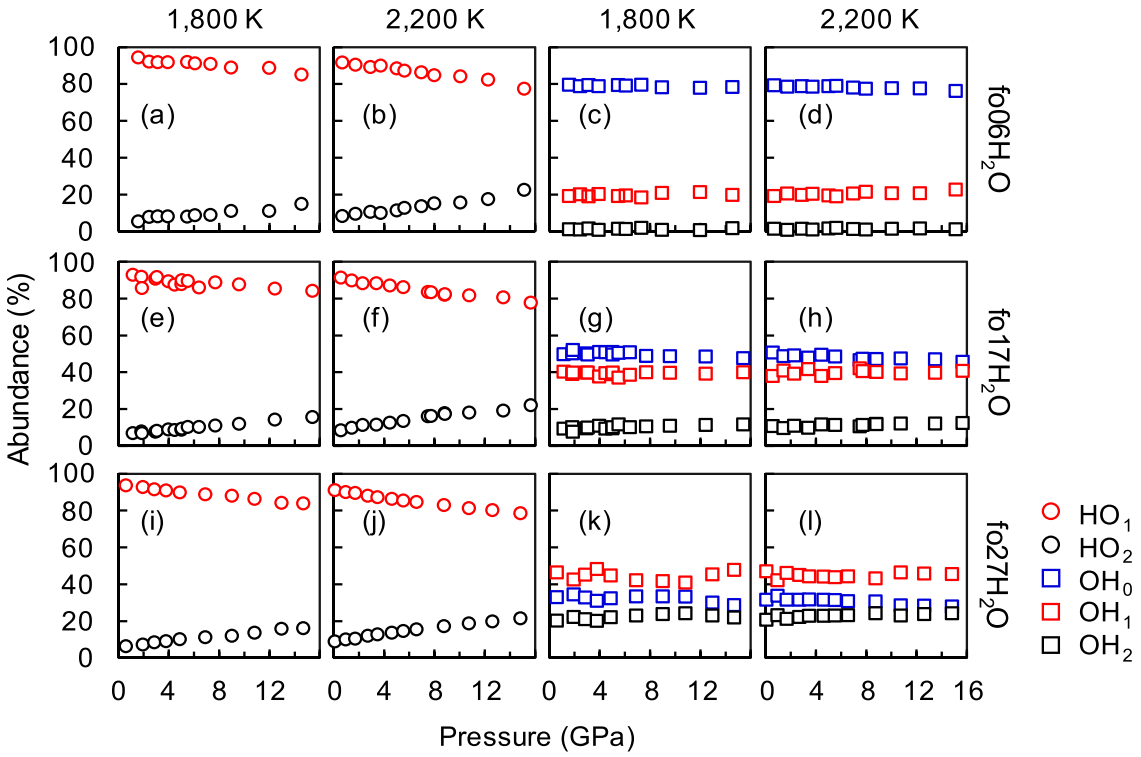

Figure 2. Hydrogen-oxygen speciation and abundance of species for different water contents in our simulations at 1,800 K (a, e, i, c, g, k) and 2,200 K (b, f, j, d, h, l). HO_1 and HO_2 indicate that a hydrogen atom is bonded to one and two oxygen atoms, respectively; OH_0, OH_1, and OH_2 indicate that an oxygen atom is bonded to zero, one, and two hydrogen atoms, respectively.

NBO (i.e., OSi_1), and an O atom with no attachment to Si atoms as free oxygen (OSi_0) (which includes groups such as molecular water and Mg-O-H) (Figure S7).

In highly polymerized melts such as SiO_2, water dissolves by reacting with bridging oxygen to form depolymerizing Si-O-H complexes (Reaction 1), whereas for depolymerized melts, there are competing water solution mechanisms that may include both network-forming and network-modifying cations. NMR and Raman measurements on depolymerized Ca,Mg-silicate melts (Xue & Kanzaki, 2004) and peralkaline melts in the Na_2O-SiO_2-H_2O system (Mysen & Cody, 2005) have been interpreted in terms of Ca-O-H and Na-O-H complexes playing a critical role in polymerizing the melt. Similarly, in the Mg_2SiO_4-H_2O systems, the Mg cations may be scavenged from their network-modifying role in anhydrous melts to form Mg-O-H complexes (Reaction 2). If Reaction 2 is *P*-dependent, the equilibrium proceeds toward one side upon compression. When the reaction proceeds to the right, the relative proportion of the Si-O-Si complexes (i.e., the degree of melt polymerization) increases which potentially provides an explanation for the observed anomalous *P*-evolution in the position of the first sharp diffraction peak (FSDP) in the structure factors determined by in situ X-ray diffraction (Yamada et al., 2007, 2011), a subject we further discuss in section 3.4.

The attachment of hydroxyl groups to Mg or Si cations is of particular importance in light of the proposed polymerization Reaction 2 which we explore by computing the relative proportions of Mg-O-H and Si-O-H complexes per oxygen, together with the abundance of Si-O-Mg and Si-O-Si groups involved (Figures 3 and S8 and Table S2). For $fo06H_2O$ melts, the network is dominantly depolymerized by the Mg cations, with almost 0.80 of the oxygen part of an Si-O-Mg complex (Figure 3). Hydrogen plays an increasingly important role in depolymerization with increasing H_2O content, triggered by both the larger number of hydrogens in the structure and the increasing O/cation (especially O/Si) ratio; for example, less than 0.10 of oxygen bridges hydrogen and silicon (Si-O-H) in the $fo06H_2O$ melts, while for $fo27H_2O$, up to 0.25 of oxygen bond as Si-O-H. A significant amount of hydroxyl groups are attached to Mg cations: The proportions of Mg-O-H in $fo06H_2O$ and $fo17H_2O$ are ~0.20 and ~0.50, and these values remain almost constant over the entire *P*-range, whereas the proportion of Mg-O-H for $fo27H_2O$ increases from 0.52 at 0 GPa to 0.66 at

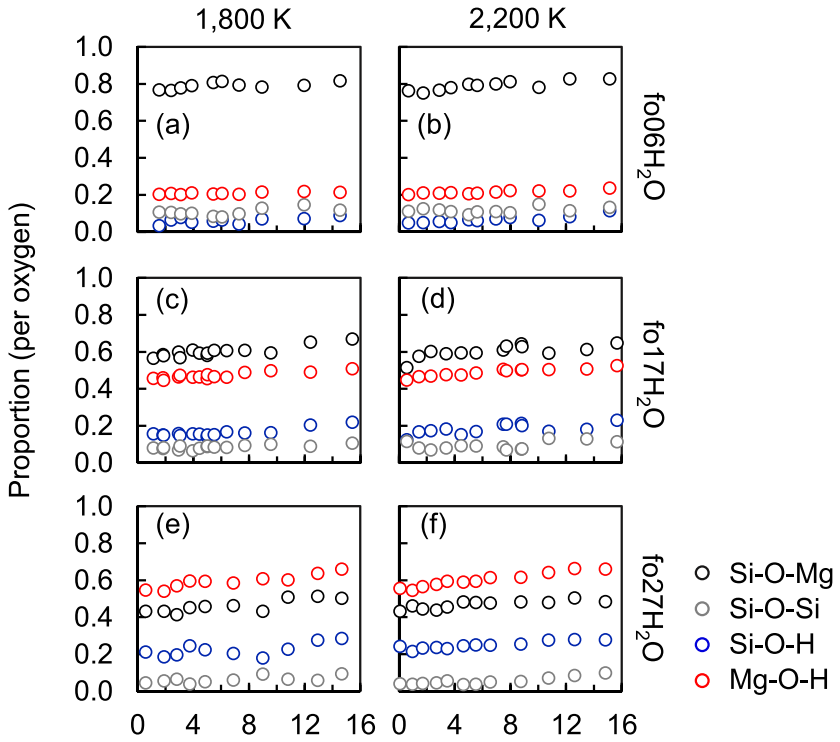

Figure 3. Proportions of Si-O-Mg, Si-O-H, Si-O-Si, and Mg-O-H complexes as a function of pressure at 1,800 K (a, c, e) and 2,200 K (b, d, f) for the different water contents in the forsterite melt. The sum of the four complexes may exceed 1 as one oxygen can be shared by different complexes (Figure S8).

15 GPa. As proposed by Yamada et al. (2011), the relative abundance of Si-O-Mg and Si-O-H decreases with P, and concurrently, the relative abundance of Si-O-Si and Mg-O-H increases according to Reaction 2. However, we find that for fo06H_2O and fo17H_2O, the effect of T and P on the relative abundance of Mg-O-H, Si-O-H, Si-O-Mg, and Si-O-Si complexes is small and for fo27H_2O, the proportion of all species experiences a gentle increase during compression as more X-O-X complexes (X represents Mg, Si, and H cations) share the same oxygen atom (Figures 3e, 3f, and S8).

Note that the sum of the four complexes (Mg-O-H, Si-O-H, Si-O-Mg, and Si-O-Si) may exceed 1 which indicates that, for example, two Si-O-Mg and Si-O-H complexes may belong to one cluster [Mg, Si]-O-H, that is, share one oxygen atom. An analysis for combined clusters (Figure S8) shows that [Si, Si]-O-Mg is the dominant type in the water-poor melt, with a proportion of 0.05–0.10. The abundance of the [Mg, Si]-O-H clusters increases with water content, and it dominates in the fo27H_2O liquid.

The Mg cation is the major cause for melt depolymerization in fo06H_2O and fo17H_2O with the Si-O-Mg complex dominant (Figures 3a–3d), and the Si-O-Mg complex remains important in fo27H_2O despite a high water concentration (Figures 3e and 3f). In line with the experimental observation that water species can be linked either to Si or metal cations in depolymerized melts (Mysen & Cody, 2005; Xue & Kanzaki, 2004), our results show that a large proportion of Mg cations are bonded to OH. While in the experimental studies the formation of free hydroxyls is interpreted as an increase in polymerization degree (e.g., Xue & Kanzaki, 2004), our results reveal that water hardly changes the depolymerizing role of Mg. The Mg cation is not scavenged from its network-modifying role by forming Mg-O-H, even though the Mg-O-H complex becomes very abundant in the water-rich system.

While NBO/Si ratios show only a marginal increase with H_2O content (Figures S9a–S9f and Table S2), the effects of water on the fractions of BO (x_{BO}), NBO (x_{NBO}), and free oxygen (x_{free-O}) is more pronounced (Figures S9g–S9i). In dry Mg_2SiO_4 (de Koker et al., 2008), $x_{BO} = 0.15$, $x_{NBO} = 0.70$, and $x_{free-O} = 0.15$ at 0 GPa, and the addition of H_2O leads to a decrease in x_{BO} and x_{NBO}, and an increase x_{free-O}, reaching

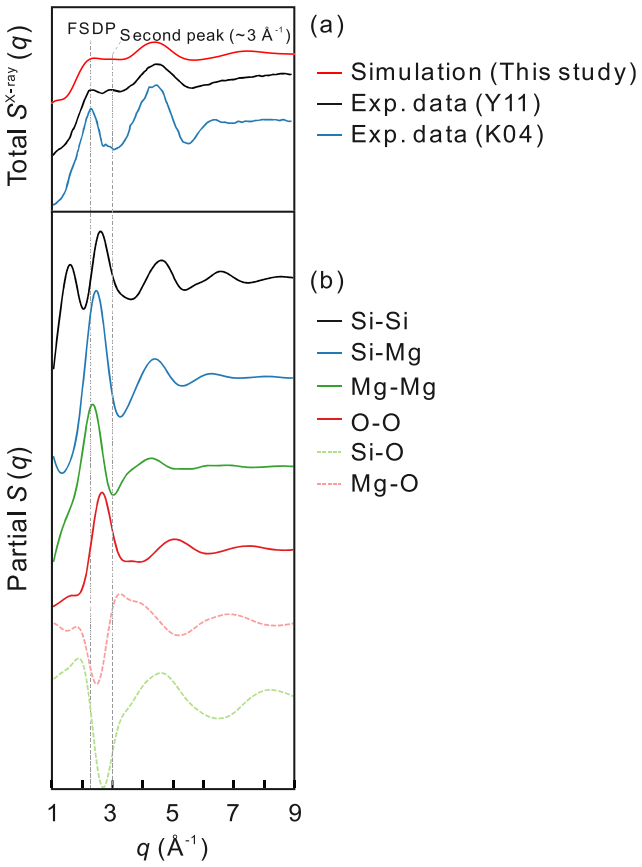

Figure 4. (a) Simulated total X-ray structure factor for hydrous Mg_2SiO_4 (1,800 K, 6.4 GPa, 16.6 wt% H_2O) in this study (red) and comparison with experimental data: hydrous Mg_2SiO_4 (1,823 K, 6.9 GPa, 20.4 wt% H_2O) from Yamada et al. (2011) (Y11, black) and vitreous Mg_2SiO_4 at ambient condition from Kohara (2004) (K04, blue). (b) Partial structure factors which have been shifted in the *y*-direction for clarity. Vertical dashed (gray) lines are a guide to the positions of the first sharp and second diffraction peak in the total structure factor.

x_{BO} = 0.06, x_{NBO} = 0.48, and x_{free-O} = 0.46 for fo27H_2O. For a given composition, x_{BO}, x_{NBO}, and x_{free-O} are not sensitive to *P* and *T*.

3.4. X-Ray Structure Factor of Hydrous Mg_2SiO_4 Melts

Our DFT-MD simulation results can be compared directly to experiments by calculating the scattering structure factor. We compute partial structure factors $S_{\alpha\beta}(q)$ between species α and β from the Fourier transform of the corresponding partial pair distribution function by means of

$$S_{\alpha\beta}(q) = \delta_{\alpha\beta} + 4\pi\rho\left(c_\alpha c_\beta\right)^{1/2}\int_0^\infty r^2\left[g_{\alpha\beta}(r) - 1\right]\frac{\sin(qr)}{qr}\,dr, \quad (5)$$

where $c_{\alpha(\beta)} = N_{\alpha(\beta)}/N$ is the concentration of $\alpha(\beta)$ species with $\alpha,\beta \in$ {Si, Mg, O, H} (Gutiérrez & Johansson, 2002). The total X-ray scattering structure factor can be obtained from the partial structure factors by weighting them with X-ray form factors $f_\alpha(s)$ (Winkler et al., 2004):

$$S^{\text{X-ray}}(q) = \frac{N}{\sum_\alpha N_\alpha f_\alpha^2(s)\sum_{\alpha\beta} f_\alpha(s) f_\beta(s) S_{\alpha\beta}(q).} \quad (6)$$

The cation-cation (i.e., Si-Si, Si-Mg, and Mg-Mg) and anion-anion correlations (i.e., O-O) have positive contributions to the FSDP, whereas the cation-anion correlations (i.e., Si-O and Mg-O) have negative contributions. Due to the poor X-ray scattering properties of hydrogen, H-H, O-H, Mg-H, and Si-H do not contribute to the X-ray structure factor.

For fo17H_2O, we compare the results of the dominant partial $S(q)$ and $S^{\text{X-ray}}(q)$ at 6.4 GPa and 1,800 K (Figure 4) with the experimental data for dry glassy Mg_2SiO_4 (Kohara, 2004) and hydrous liquid Mg_2SiO_4 (Yamada et al., 2011). The structure factor and the FSDP, in particular, provide information on the intermediate-range order with a spacing larger than the interatomic distance (Elliott, 1991). The position of the FSDP at zero *P* is predicted at $q \sim 2.18$ Å^{-1} for fo06H_2O, comparable to that in vitreous Mg_2SiO_4 (Kohara, 2004) and shifts to $q \sim 2.22$ Å^{-1} for fo17H_2O and to $q \sim 2.32$ Å^{-1} for fo27H_2O, representing a general trend of a larger q for the FSDP with increasing H_2O content at constant *P*. This is consistent with experimental observations regarding the effect of hydrogen (Zotov et al., 1996, 1992) and the alkali elements K and Na (Du & Corrales, 2006) on the FSDP position in melts and glasses. We find a second peak close to the FSDP at ~3.0 Å^{-1}, consistent with the one observed in experiments (Yamada et al., 2011). This second peak is correlated with S_{MgO}.

The FSDP of glassy forsterite (Mg_2SiO_4) determined by X-ray diffraction is located at $q \sim 2.2$–2.3 Å^{-1} (Kohara, 2004; Kohara et al., 2011), larger than for $MgSiO_3$ enstatite glass with $q \sim 2.1$–2.2 Å^{-1} (Funamori et al., 2004; Kohara et al., 2011). In hydrous Mg_2SiO_4 melts, H interrupts the covalent network connectivity in a similar way as Mg and should therefore lead to a decrease of medium-range order, resulting in a shift of FSDP to larger q values. By contrast, the measured FSDP position ($q \sim 2.0$ Å^{-1}) in hydrous Mg_2SiO_4 melt (Yamada et al., 2011) is at lower q than that in anhydrous Mg_2SiO_4 glass (Kohara, 2004; Kohara et al., 2011), and similarly, the FSDP position in hydrous $MgSiO_3$ melt (Yamada et al., 2011) is at lower q than that in dry $MgSiO_3$ melt (Funamori et al., 2004; Kohara et al., 2011) at $P \sim 6$ GPa. These results seem to be at odds with the previous experimental conclusion for hydrous glass (Zotov et al., 1996, 1992). For a quantitative comparison of the FSDP positions from different experiments, one needs to take *T*-effect into account, however.

Our DFT-MD results suggest that the FSDP position in hydrous Mg_2SiO_4 is positively correlated to H_2O content and *P* (Figure S10) and there is no evidence to support an increasing degree of melt polymerization with *P* to 15 GPa and H_2O content to 27 wt%. We emphasize that the variation of water content and Mg/Si ratio of the melts may lead to different conclusions. Melts studied by Xue and Kanzaki (2004) contain less MgO

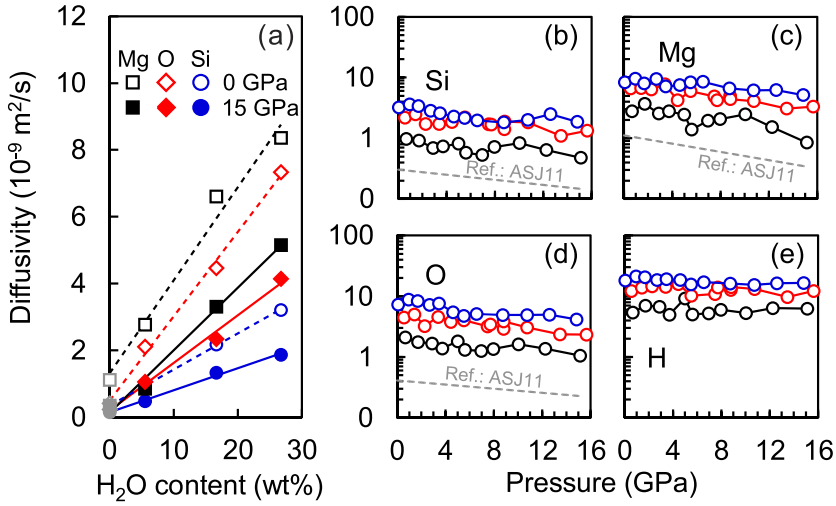

Figure 5. Elemental diffusivities in hydrous Mg_2SiO_4 melt at 2,200 K. (a) Diffusion coefficients for Mg, O, and Si as a function of water content. (b–e) Diffusion coefficients for Mg, O, Si, and H as a function of pressure in fo06H_2O (black), fo17H_2O (red), and fo27H_2O (blue). Results for dry Mg_2SiO_4 melt are from Adjaoud et al. (2011) (ASJ11, gray in a–d). The uncertainty of diffusivity is in the range of 20–30% (Figure S11).

compared to the Mg_2SiO_4 melt considered in this study; although the Mg_2SiO_4 melts studied previously (Yamada et al., 2007, 2011) are water-rich, the diamond capsule with platinum caps used in their experiments may not fully retain water. The anomaly in the FSDP position with respect to P observed by Yamada et al. (2011), if true, more likely occurs at water-poor conditions. This highlights the need to conduct further simulations on water-poor and less depolymerized melts such as $MgSiO_3$.

3.5. Diffusivities

The diffusion constants of a species α in the liquid can be calculated from the MSD using the Einstein relation, $D_\alpha = \lim_{t\to\infty} \frac{\mathrm{MSD}_\alpha}{6t}$. As deuterium mass was assigned to hydrogen atoms, the actual calculations of the dynamic properties are performed for deuterium instead of hydrogen. Hydrogen diffusivity (D_H) is larger than deuterium diffusivity (D_D) with a D_H/D_D ratio of ~1.2 for the one example (fo27H_2O at 0 GPa and 1,800 K) we have explored explicitly (Figure S1). To determine the uncertainty on diffusivity, we performed multiple simulations ($n = 50$ runs) starting from the same configuration but different initialized velocities both at 1,800 and 2,200 K, following the suggestions of Maginn et al. (2019). For each trajectory, we performed a linear fitting of MSD-t curve in a time range between 1 and 10 ps and obtained a distribution of diffusivity (expressed as histograms in Figure S11). The standard deviation of this distribution for diffusivity is in the range of 30–40% at 1,800 K and 20–30% at 2,200 K. Simulations at high T have faster dynamics and better sampling whereas those at lower T sample fewer linear diffusion events and therefore are associated with larger statistical uncertainty.

As expected, the computed diffusivity sequence is $D_{H/D} > D_{Mg} \geq D_O > D_{Si}$ for all conditions considered (Figure 5). Hydrogen diffuses fastest in the melts; Si is the slowest species as it is confined within SiO_n polyhedra; network modifiers (i.e., Mg) are weakly bonded to oxygen and therefore relatively mobile. Pressure leads to decreased mobility of species and consequently to smaller D_α-values for Si, Mg, and O, while H/D does not experience a significant reduction in D_α over the entire P-range considered. Compared to dry Mg_2SiO_4 liquid in previous molecular dynamics simulations (Adjaoud et al., 2011; Ghosh & Karki, 2011), the diffusion coefficients of all species (Si, Mg, and O) are larger over the entire P-range (Figures 5b–5e). Self-diffusion coefficients increase approximately linearly with water content (C_{H_2O} in wt%) both at ambient and high P (Figure 5a).

Mass transport properties of liquids, such as diffusivity, are well known to be strongly related to melt structure and can therefore be used as an indicator for changes in it (e.g., Posner et al., 2017). Assuming that there is a structural change in response to P as proposed by Yamada et al. (2007, 2011) in hydrous Mg_2SiO_4 melts

(Reaction 2), an anomaly in diffusivity would be expected. However, our predicted self-diffusion coefficients display a typical *P*-induced decrease for depolymerized melts (Ghosh & Karki, 2017; Mookherjee et al., 2008; Ni et al., 2015), supporting the interpretation that H_2O dissolution does not cause an increase in the degree of polymerization of the network structure for mafic-ultramafic melts (here Mg_2SiO_4).

4. Implications for the Gravitational Stability of Hydrous Melts Near the MTZ

The MTZ is potentially a significant water reservoir in the deep Earth due to the high solubility of water in its dominant minerals, wadsleyite and ringwoodite (Inoue et al., 1995; Kohlstedt et al., 1996; Kudoh et al., 1996). When material moves away from the MTZ, dehydration melting may occur as the amount of water held in MTZ minerals probably exceeds the saturation limit of the phase assemblages in the upper and lower mantle (Bercovici & Karato, 2003; Schmandt et al., 2014). Moreover, melts are unlikely to be generated in the dry-peridotite system at comparable conditions, as the solidus *T* increases significantly with *P* (Takahashi, 1986; Zhang & Herzberg, 1994). The origin of low-velocity zones near the MTZ has therefore been widely attributed to hydrous partial melting.

The gravitational stability of melt in the deep mantle is primarily controlled by the ρ-contrast between silicate melt and surrounding peridotite rock, which depend primarily on *T* and composition. Temperatures at which partial melting occurs at the 410-km and 660-km seismic discontinuities are estimated to be in the range of ~1,800–1,900 K (Chust et al., 2017; Ito & Katsura, 1989), which is lower than *T* used in most previous determinations of melt ρ by experiments (e.g., Matsukage et al., 2005; Sakamaki et al., 2006) and especially simulations (e.g., Bajgain et al., 2015; Mookherjee et al., 2008).

The generation of melt in ultramafic composition with a ratio of Mg/Si = 2 used in our simulations may appear unlikely in the mantle. However, melts produced by incongruent melting of peridotite move to ultramafic compositions with increasing *P*, and the ratio (Mg + Fe)/Si is approaching a value of 2 or larger for hydrous compositions (Inoue, 1994; Kawamoto, 2004; Kawamoto & Holloway, 1997) at MTZ conditions, making our results relevant for considerations of partial melting there. Using the compressibility behavior of dissolved water in silicate melt (Figure 1 and Table 1) and the compressibility of the dry silicate liquid, ρ of hydrous silicate melts can be estimated based on our results. We examine ρ of melts with idealized compositions of Mg_2SiO_4 and $(Mg_{1-x}Fe_x)_2SiO_4$, and a multicomponent realistic peridotitic melt at 1,800 K, and compare them with ρ-profiles of seismic models in and around the MTZ, especially just above the 410-km seismic discontinuity.

We determine the density of Mg_2SiO_4-based melts by combining the compressibility parameters of dry Mg_2SiO_4 melt (de Koker et al., 2008) with those of the water component in silicate melt from our DFT-MD results (Tables 1 and S3). Calculated ρ of both dry and hydrous Mg_2SiO_4 melts are significantly lower than ρ-values of seismic models (Figure 6a). For instance, ρ of dry Mg_2SiO_4 melt is smaller by ~10–12% compared to the Preliminary Reference Earth Model (PREM) (Dziewonski & Anderson, 1981) and the average value of the 99 pyrolite models from Monte Carlo inversion for mantle structure (99PREFum) (Cammarano et al., 2005) throughout the MTZ; above the 410-km seismic discontinuity, they are lower by ~6% and ~10% compared to these profiles, respectively.

A ρ-crossover between melts and crystals is only possible by taking the effect of the iron component into account. Under anhydrous conditions (Mibe et al., 2006), a distribution coefficient $K_D^{FeO/MgO} = (FeO/MgO)_{olivine}/(FeO/MgO)_{melt}$~0.3 was estimated between 5 and 13 GPa, and while H_2O may affect $K_D^{FeO/MgO}$ values, melting experiments of water-saturated peridotite show a similar value of $K_D^{FeO/MgO}$~0.26 at 11 GPa (Kawamoto & Holloway, 1997). Using $K_D^{FeO/MgO} = 0.3$ and assuming the melt is in equilibrium with a pyrolite mantle which has an Mg# of 89 (i.e., the molar ratio of Mg/(Mg + Fe) × 100), the hydrous melt has an Mg# of 71. Using a Vegard-type mixing model in which the molar *V* of a silicate melt is given by a linear combination of partial molar *V* of MgO and FeO oxide components using the ratio from Lange and Carmichael (1987) and appropriate molar weights, we estimate ρ_0 for $(Mg_{0.71}Fe_{0.29})_2SiO_4$ melt at 1,800 K (Table S3). While ideal mixing of volumes has proven to be a reliable method of determining ρ_0 of silicate melts (Lange & Carmichael, 1987), there is evidence that the partial molar volume FeO ($\overline{V}_{FeO}$) varies with composition (e.g., Guo et al., 2014; Thomas & Asimow, 2013), with negligible effect on ρ_0 for the melt

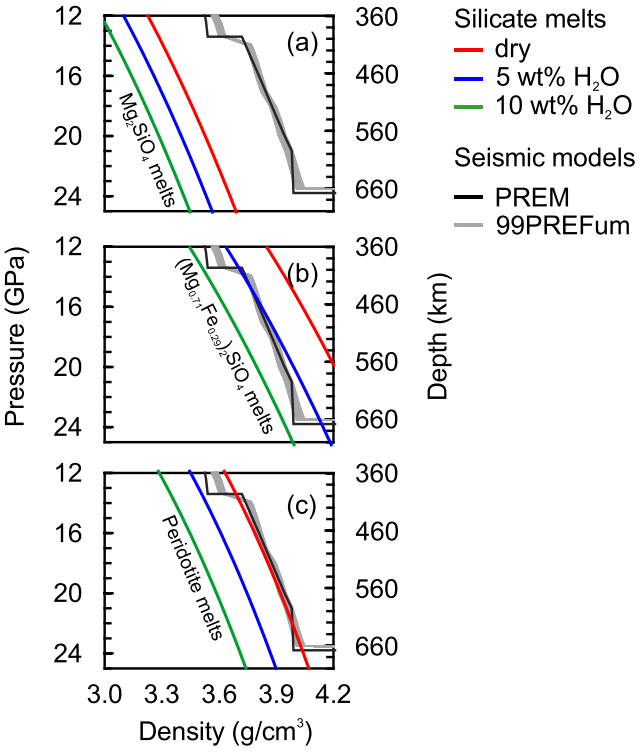

Figure 6. (a) Density of silicate melts with idealized compositions of Mg_2SiO_4 (a), $(Mg_{0.71}Fe_{0.29})_2SiO_4$ (b), and a multicomponent peridotite melt (c). Density of melts with 0, 5, and 10 wt% H_2O are shown by red, blue, and green colors, respectively. The Preliminary Reference Earth Model (PREM) (Dziewonski & Anderson, 1981) (black line) and the 99 pyrolite models (99PREFum) (Cammarano et al., 2005) (gray shaded area) are included for comparison.

composition considered here. For consistency with previous work (Jing & Karato, 2008), we use the linear mixing approach. We further assume that values of K_T and K' of $(Mg_{0.71}Fe_{0.29})_2SiO_4$ melt are the same as those used for Mg_2SiO_4, insensitive to change of Mg# (Jing & Karato, 2008). For 5 wt% of H_2O, this melt follows the seismic ρ-profile throughout the MTZ to first order (Figure 6b) but is positively buoyant above both the 410-km and 660-km seismic discontinuities. The critical water content—at which the melt is neutrally buoyant relative to mantle peridotite—at 13.4 GPa and 23.8 GPa is ~9 wt%.

Finally, we evaluate ρ of hydrous melt with a representative mantle composition by using ρ_{H_2O} from our DFT-MD simulations (Tables 1 and S3) in conjunction with ρ of (dry) peridotitic melt. For that, we use an experimental composition in the CaO-MgO-Al_2O_3-SiO_2 pyrolite system with 2 wt% H_2O (Litasov & Ohtani, 2002)—a water content consistent with mineral viscosity considerations by Fei et al. (2017)—that results in a partial melt composition of 49.2 wt% SiO_2, 3.4 wt% Al_2O_3, 34.5 wt% MgO, and 12.9 wt% CaO. Other oxide components such as K_2O and Na_2O are not considered because of their low concentrations and therefore negligible effects on melt ρ (Freitas et al., 2017). To include FeO in the melt chemistry, an Mg# of 71 was used following the arguments given above, and we estimate ρ_0 based on partial molar volume ratios by Lange and Carmichael (1987). We ignore non-ideal mixing effects between SiO_2, Al_2O_3, FeO, MgO, and CaO expressed by an excess volume term (e.g., Xin et al., 2019), corresponding to the possible interactions between them, as it results in only a marginal shift of ρ_0. For compressibility of the dry peridotitic melt, we use data by Ohtani and Maeda (2001) and Sakamaki et al. (2009) (Table S3). This melt model results in ρ-profiles at MTZ conditions shown in Figure 6c: The dry peridotite closely follows the seismological ρ-profile throughout the MTZ, and the critical water content is ~4 wt% H_2O just above the 410-km seismic discontinuity. This water content is lower than estimated previously, for example, 6–7 wt% H_2O in Matsukage et al. (2005), who have adopted $\overline{V}_{H_2O} < 8$ cm^3/mol, at the low end of their experimental constraints and smaller than the values found in our study (Figure 1d).

Consequently, the key consideration for the fate of hydrous partial melts formed at the edges of the MTZ is the H_2O content. Both melting experiments (Litasov & Ohtani, 2002; Zhang et al., 2017) and thermodynamic modeling (Hirschmann et al., 2009; Novella et al., 2017) suggest that partial melts above the 410-km seismic discontinuity form with a minimum of ~15 wt% dissolved H_2O, which is much larger than the critical water content at the 410-km (~4 wt%) and 660-km seismic discontinuities (~0 wt%) estimated here. This small critical H_2O content suggests that water is a significant buoyancy source for triggering deep plumes ascending from lowermost upper mantle storage as imaged by seismic tomography (Tian et al., 2016; Xia et al., 2016; Zhao et al., 2009).

5. Conclusion

We have simulated hydrous Mg_2SiO_4 melts with 5.5–26.7 wt% H_2O using ab initio molecular dynamics methods to study their structure, density, and dynamic properties over *P-T* conditions of the upper mantle and the mantle transition zone. Despite high water contents in the melts, the Si-O-Mg complex constitutes a large proportion of the X-O-X complexes (X represents Mg, Si, and H cations), and it is the major cause for depolymerizing melt structure. Water hardly changes the depolymerization role of the Mg cations, even though a strong interaction between water species and Mg can be observed from both our simulations and previous spectroscopy studies (e.g., Xue & Kanzaki, 2004). However, our results based on combined evidence from static and dynamic properties of the melt do not support the hypothesis inferred from NMR data and X-ray structure factors that ultramafic magmas may be polymerized by the presence of dissolved water.

This result is quite different from the polymerizing effect of CO_2 on the melt network shown in previous simulations (Moussallam et al., 2016).

We have examined the buoyancy stability of water-rich silicate melts generated through dehydration melting near the mantle transition zone. Taking iron partitioning into account, the critical water content at which hydrous melts have the same density as the mantle (density crossover) is less than 10 wt% despite iron enrichment in the melt. Therefore, water-rich melts cannot experience long-term gravitational stability in the mantle transition zone and its vicinity. Low velocity zones imaged near the 410-km and 660-km seismic discontinuities are likely transient features resulting from continuous downward/upward flow across the transition zone boundaries.

Data Availability Statement

Computations were performed at the Leibniz Supercomputing Center of the Bavarian Academy of Sciences and the Humanities. The Vienna Ab Initio Simulation Package (VASP) is proprietary software for which licenses are issued online (https://www.vasp.at/). In compliance with the journal's FAIR data availability requirements, the simulation files are described in computational methods and are archived in Figshare (https://doi.org/10.6084/m9.figshare.11803113).

Acknowledgments
We thank Eiji Ohtani for his very helpful and constructive comments on this work and manuscript. L.Y. was supported by the JSPS Japanese–German Graduate Externship and the International Joint Graduate Program in Earth and Environmental Science, Tohoku University, and the collaboration between Bayerisches Geoinstitut and Tohoku University was facilitated by the German Science Foundation (Deutsche Forschungsgemeinschaft, DFG) through the International Research and Training Group "Deep Earth Volatile Cycles" (GRK 2156). Open access funding enabled and organized by Projekt DEAL.

References

Adjaoud, O., Steinle-Neumann, G., & Jahn, S. (2011). Transport properties of Mg_2SiO_4 liquid at high pressure: Physical state of a magma ocean. *Earth and Planetary Science Letters*, *312*(3–4), 463–470. https://doi.org/10.1016/j.epsl.2011.10.025

Agee, C. B. (2008). Static compression of hydrous silicate melt and the effect of water on planetary differentiation. *Earth and Planetary Science Letters*, *265*(3–4), 641–654. https://doi.org/10.1016/j.epsl.2007.11.010

Alex Song, T.-R., Helmberger, D. V., & Grand, S. P. (2004). Low-velocity zone atop the 410-km seismic discontinuity in the northwestern United States. *Nature*, *427*(6974), 530–533. https://doi.org/10.1038/nature02231

Aubaud, C., Hauri, E. H., & Hirschmann, M. M. (2004). Hydrogen partition coefficients between nominally anhydrous minerals and basaltic melts. *Geophysical Research Letters*, *31*, L20611. https://doi.org/10.1029/2004GL021341

Bajgain, S. K., Ghosh, D. B., & Karki, B. B. (2015). Structure and density of basaltic melts at mantle conditions from first-principles simulations. *Nature Communications*, *6*(1), 8578. https://doi.org/10.1038/ncomms9578

Bercovici, D., & Karato, S. (2003). Whole-mantle convection and the transition-zone water filter. *Nature*, *425*(6953), 39–44. https://doi.org/10.1038/nature01918

Cammarano, F., Deuss, A., Goes, S., & Giardini, D. (2005). One-dimensional physical reference models for the upper mantle and transition zone: Combining seismic and mineral physics constraints. *Journal of Geophysical Research*, *110*, B01306. https://doi.org/10.1029/2004JB003272

Chust, T. C., Steinle-Neumann, G., Dolejš, D., Schuberth, B. S. A., & Bunge, H. P. (2017). MMA-EoS: A computational framework for mineralogical thermodynamics. *Journal of Geophysical Research: Solid Earth*, *122*, 9881–9920. https://doi.org/10.1002/2017JB014501

de Koker, N. P., Stixrude, L., & Karki, B. B. (2008). Thermodynamics, structure, dynamics, and freezing of Mg_2SiO_4 liquid at high pressure. *Geochimica et Cosmochimica Acta*, *72*(5), 1427–1441. https://doi.org/10.1016/j.gca.2007.12.019

Dingwell, D. B., Romano, C., & Hess, K.-U. (1996). The effect of water on the viscosity of a haplogranitic melt under *P-T-X* conditions relevant to silicic volcanism. *Contributions to Mineralogy and Petrology*, *124*(1), 19–28. https://doi.org/10.1007/s004100050170

Du, J., & Corrales, L. R. (2006). Compositional dependence of the first sharp diffraction peaks in alkali silicate glasses: A molecular dynamics study. *Journal of Non-Crystalline Solids*, *352*(30–31), 3255–3269. https://doi.org/10.1016/j.jnoncrysol.2006.05.025

Dziewonski, A. M., & Anderson, D. L. (1981). Preliminary reference Earth model. *Physics of the Earth and Planetary Interiors*, *25*(4), 297–356. https://doi.org/10.1016/0031-9201(81)90046-7

Elliott, S. R. (1991). Medium-range structural order in covalent amorphous solids. *Nature*, *354*(6353), 445–452. https://doi.org/10.1038/354445a0

Fei, H., Yamazaki, D., Sakurai, M., Miyajima, N., Ohfuji, H., Katsura, T., & Yamamoto, T. (2017). A nearly water-saturated mantle transition zone inferred from mineral viscosity. *Science Advances*, *3*(6), e1603024. https://doi.org/10.1126/sciadv.1603024

Freitas, D., Manthilake, G., Schiavi, F., Chantel, J., Bolfan-Casanova, N., Bouhifd, M. A., & Andrault, D. (2017). Experimental evidence supporting a global melt layer at the base of the Earth's upper mantle. *Nature Communications*, *8*(1), 2186. https://doi.org/10.1038/s41467-017-02275-9

Funamori, N., Yamamoto, S., Yagi, T., & Kikegawa, T. (2004). Exploratory studies of silicate melt structure at high pressures and temperatures by in situ X-ray diffraction. *Journal of Geophysical Research*, *109*, B03203. https://doi.org/10.1029/2003JB002650

Gaillard, F. (2004). Laboratory measurements of electrical conductivity of hydrous and dry silicic melts under pressure. *Earth and Planetary Science Letters*, *218*(1–2), 215–228. https://doi.org/10.1016/S0012-821X(03)00639-3

Gavrilenko, M., Krawczynski, M., Ruprecht, P., Li, W., & Catalano, J. G. (2019). The quench control of water estimates in convergent margin magmas. *American Mineralogist*, *104*(7), 936–948. https://doi.org/10.2138/am-2019-6735

Ghosh, D. B., Bajgain, S. K., Mookherjee, M., & Karki, B. B. (2017). Carbon-bearing silicate melt at deep mantle conditions. *Scientific Reports*, *7*(1), 848. https://doi.org/10.1038/s41598-017-00918-x

Ghosh, D. B., & Karki, B. B. (2011). Diffusion and viscosity of Mg_2SiO_4 liquid at high pressure from first-principles simulations. *Geochimica et Cosmochimica Acta*, *75*(16), 4591–4600. https://doi.org/10.1016/j.gca.2011.05.030

Ghosh, D. B., & Karki, B. B. (2017). Transport properties of carbonated silicate melt at high pressure. *Science Advances*, *3*(12), e1701840. https://doi.org/10.1126/sciadv.1701840

Guo, X., Lange, R. A., & Ai, Y. (2014). Density and sound speed measurements on model basalt (An-Di-Hd) liquids at one bar: New constraints on the partial molar volume and compressibility of the FeO component. *Earth and Planetary Science Letters*, *388*, 283–292. https://doi.org/10.1016/j.epsl.2013.12.005

Gutiérrez, G., & Johansson, B. (2002). Molecular dynamics study of structural properties of amorphous Al_2O_3. *Physical Review B*, *65*(10), 104,202. https://doi.org/10.1103/PhysRevB.65.104202

Hirschmann, M. M., Tenner, T., Aubaud, C., & Withers, A. C. (2009). Dehydration melting of nominally anhydrous mantle: The primacy of partitioning. *Physics of the Earth and Planetary Interiors*, *176*(1–2), 54–68. https://doi.org/10.1016/j.pepi.2009.04.001

Hong, Q. J., & Van De Walle, A. (2013). Solid-liquid coexistence in small systems: A statistical method to calculate melting temperatures. *The Journal of Chemical Physics*, *139*(9), 094114. https://doi.org/10.1063/1.4819792

Hoover, W. G. (1985). Canonical dynamics: Equilibrium phase-space distributions. *Physical Review A*, *31*(3), 1695–1697. https://doi.org/10.1103/PhysRevA.31.1695

Hui, H., & Zhang, Y. (2007). Toward a general viscosity equation for natural anhydrous and hydrous silicate melts. *Geochimica et Cosmochimica Acta*, *71*(2), 403–416. https://doi.org/10.1016/j.gca.2006.09.003

Inoue, T. (1994). Effect of water on melting phase relations and melt composition in the system Mg_2SiO_4-$MgSiO_3$-H_2O up to 15 GPa. *Physics of the Earth and Planetary Interiors*, *85*(3–4), 237–263. https://doi.org/10.1016/0031-9201(94)90116-3

Inoue, T., Yurimoto, H., & Kudoh, Y. (1995). Hydrous modified spinel, $Mg_{1.75}SiH_{0.5}O_4$: A new water reservoir in the mantle transition region. *Geophysical Research Letters*, *22*(2), 117–120. https://doi.org/10.1029/94GL02965

Ito, E., & Katsura, T. (1989). A temperature profile of the mantle transition zone. *Geophysical Research Letters*, *16*(5), 425–428. https://doi.org/10.1029/GL016i005p00425

Jing, Z., & Karato, S. (2008). Compositional effect on the pressure derivatives of bulk modulus of silicate melts. *Earth and Planetary Science Letters*, *272*(1–2), 429–436. https://doi.org/10.1016/j.epsl.2008.05.013

Jing, Z., & Karato, S. (2012). Effect of H_2O on the density of silicate melts at high pressures: Static experiments and the application of a modified hard-sphere model of equation of state. *Geochimica et Cosmochimica Acta*, *85*, 357–372. https://doi.org/10.1016/j.gca.2012.03.001

Karki, B. B., & Stixrude, L. (2010). First-principles study of enhancement of transport properties of silica melt by water. *Physical Review Letters*, *104*(21), 215901. https://doi.org/10.1103/PhysRevLett.104.215901

Karki, B. B., Zhang, J., & Stixrude, L. (2013). First principles viscosity and derived models for MgO-SiO_2 melt system at high temperature. *Geophysical Research Letters*, *40*, 94–99. https://doi.org/10.1029/2012GL054372

Kawamoto, T. (2004). Hydrous phase stability and partial melt chemistry in H_2O-saturated KLB-1 peridotite up to the uppermost lower mantle conditions. *Physics of the Earth and Planetary Interiors*, *143*, 387–395. https://doi.org/10.1016/j.pepi.2003.06.003

Kawamoto, T., & Holloway, J. R. (1997). Melting temperature and partial melt chemistry of H_2O-saturated mantle peridotite to 11 gigapascals. *Science*, *276*(5310), 240–243. https://doi.org/10.1126/science.276.5310.240

Kohara, S. (2004). Glass formation at the limit of insufficient network formers. *Science*, *303*(5664), 1649–1652. https://doi.org/10.1126/science.1095047

Kohara, S., Akola, J., Morita, H., Suzuya, K., Weber, J. K. R., Wilding, M. C., & Benmore, C. J. (2011). Relationship between topological order and glass forming ability in densely packed enstatite and forsterite composition glasses. *Proceedings of the National Academy of Sciences*, *108*(36), 14,780–14,785. https://doi.org/10.1073/pnas.1104692108

Kohlstedt, D. L., Keppler, H., & Rubie, D. C. (1996). Solubility of water in the α, β and γ phases of $(Mg,Fe)_2SiO_4$. *Contributions to Mineralogy and Petrology*, *123*(4), 345–357. https://doi.org/10.1007/s004100050161

Kresse, G., & Furthmüller, J. (1996). Efficient iterative schemes for ab initio total-energy calculations using a plane-wave basis set. *Physical Review B*, *54*(16), 11,169–11,186. https://doi.org/10.1103/PhysRevB.54.11169

Kresse, G., & Hafner, J. (1993). Ab initio molecular dynamics for liquid metals. *Physical Review B*, *47*(1), 558–561. https://doi.org/10.1103/PhysRevB.47.558

Kresse, G., & Joubert, D. (1999). From ultrasoft pseudopotentials to the projector augmented-wave method. *Physical Review B*, *59*(3), 1758–1775. https://doi.org/10.1103/PhysRevB.59.1758

Kudoh, Y., Inoue, T., & Arashi, H. (1996). Structure and crystal chemistry of hydrous wadsleyite, $Mg_{1.75}SiH_{0.5}O_4$: Possible hydrous magnesium silicate in the mantle transition zone. *Physics and Chemistry of Minerals*, *23*, 461–469. https://doi.org/10.1007/bf00202032

Kuritani, T., Xia, Q.-K., Kimura, J.-I., Liu, J., Shimizu, K., Ushikubo, T., et al. (2019). Buoyant hydrous mantle plume from the mantle transition zone. *Scientific Reports*, *9*(1), 6549. https://doi.org/10.1038/s41598-019-43103-y

Lange, R. A., & Carmichael, I. S. E. (1987). Densities of Na_2O-K_2O-CaO-MgO-FeO-Fe_2O_3-Al_2O_3-TiO_2-SiO_2 liquids: New measurements and derived partial molar properties. *Geochimica et Cosmochimica Acta*, *51*(11), 2931–2946. https://doi.org/10.1016/0016-7037(87)90368-1

Lee, S. K., Mosenfelder, J. L., Park, S. Y., Lee, A. C., & Asimow, P. D. (2020). Configurational entropy of basaltic melts in Earth's mantle. *Proceedings of the National Academy of Sciences*, *117*(36), 21,938–21,944. https://doi.org/10.1073/pnas.2014519117

Litasov, K., & Ohtani, E. (2002). Phase relations and melt compositions in CMAS-pyrolite-H_2O system up to 25 GPa. *Physics of the Earth and Planetary Interiors*, *134*(1–2), 105–127. https://doi.org/10.1016/S0031-9201(02)00152-8

Liu, Z., Park, J., & Karato, S. (2016). Seismological detection of low-velocity anomalies surrounding the mantle transition zone in Japan subduction zone. *Geophysical Research Letters*, *43*, 2480–2487. https://doi.org/10.1002/2015GL067097

Liu, Z., Park, J., & Karato, S. (2018). Seismic evidence for water transport out of the mantle transition zone beneath the European Alps. *Earth and Planetary Science Letters*, *482*, 93–104. https://doi.org/10.1016/j.epsl.2017.10.054

Maginn, E. J., Messerly, R. A., Carlson, D. J., Roe, D. R., & Elliott, J. R. (2019). Best practices for computing transport properties 1. Self-diffusivity and viscosity from equilibrium molecular dynamics. *Living Journal of Compuational Molecular Science*, *1*. https://doi.org/10.33011/livecoms.1.1.6324

Matsukage, K. N., Jing, Z., & Karato, S. I. (2005). Density of hydrous silicate melt at the conditions of Earth's deep upper mantle. *Nature*, *438*(7067), 488–491. https://doi.org/10.1038/nature04241

Mibe, K., Fujii, T., Yasuda, A., & Ono, S. (2006). Mg-Fe partitioning between olivine and ultramafic melts at high pressures. *Geochimica et Cosmochimica Acta*, *70*(3), 757–766. https://doi.org/10.1016/j.gca.2005.09.022

Mibe, K., Kanzaki, M., Kawamoto, T., Matsukage, K. N., Fei, Y., & Ono, S. (2007). Second critical endpoint in the peridotite-H_2O system. *Journal of Geophysical Research*, *112*, B03201. https://doi.org/10.1029/2005jb004125

Mookherjee, M., Stixrude, L., & Karki, B. (2008). Hydrous silicate melt at high pressure. *Nature*, *452*(7190), 983–986. https://doi.org/10.1038/nature06918

Moussallam, Y., Florian, P., Corradini, D., Morizet, Y., Sator, N., Vuilleumier, R., et al. (2016). The molecular structure of melts along the carbonatite-kimberlite-basalt compositional joint: CO_2 and polymerisation. *Earth and Planetary Science Letters*, *434*, 129–140. https://doi.org/10.1016/j.epsl.2015.11.025

Mysen, B., & Cody, G. (2005). Solution mechanisms of H_2O in depolymerized peralkaline melts. *Geochimica et Cosmochimica Acta*, *69*(23), 5557–5566. https://doi.org/10.1016/j.gca.2005.07.020

Mysen, B., & Richet, P. (2005). *Silicate glasses and melts: Properties and structure* (1st ed.). Amsterdam, Netherlands: Elsevier.

Mysen, B., & Wheeler, K. (2000). Solubility behavior of water in haploandesitic melts at high pressure and high temperature. *American Mineralogist*, *85*(9), 1128–1142. https://doi.org/10.2138/am-2000-8-903

Ni, H., Hui, H., & Steinle-Neumann, G. (2015). Transport properties of silicate melts. *Reviews of Geophysics*, *53*(3), 715–744. https://doi.org/10.1002/2015RG000485

Ni, H., Keppler, H., & Behrens, H. (2011). Electrical conductivity of hydrous basaltic melts: Implications for partial melting in the upper mantle. *Contributions to Mineralogy and Petrology*, *162*(3), 637–650. https://doi.org/10.1007/s00410-011-0617-4

Novella, D., Dolejš, D., Myhill, R., Pamato, M. G., Manthilake, G., & Frost, D. J. (2017). Melting phase relations in the systems Mg_2SiO_4-H_2O and $MgSiO_3$-H_2O and the formation of hydrous melts in the upper mantle. *Geochimica et Cosmochimica Acta*, *204*, 68–82. https://doi.org/10.1016/j.gca.2016.12.042

Novella, D., Frost, D. J., Hauri, E. H., Bureau, H., Raepsaet, C., & Roberge, M. (2014). The distribution of H_2O between silicate melt and nominally anhydrous peridotite and the onset of hydrous melting in the deep upper mantle. *Earth and Planetary Science Letters*, *400*, 1–13. https://doi.org/10.1016/j.epsl.2014.05.006

Ochs, F. A., & Lange, R. A. (1999). The density of hydrous magmatic liquids. *Science*, *283*(5406), 1314–1317. https://doi.org/10.1126/science.283.5406.1314

Ohtani, E., & Kumazawa, M. (1981). Melting of forsterite Mg_2SiO_4 up to 15 GPa. *Physics of the Earth and Planetary Interiors*, *27*(1), 32–38. https://doi.org/10.1016/0031-9201(81)90084-4

Ohtani, E., & Maeda, M. (2001). Density of basaltic melt at high pressure and stability of the melt at the base of the lower mantle. *Earth and Planetary Science Letters*, *193*(1–2), 69–75. https://doi.org/10.1016/S0012-821X(01)00505-2

Pan, D., & Galli, G. (2016). The fate of carbon dioxide in water-rich fluids under extreme conditions. *Science Advances*, *2*(10), e1601278. https://doi.org/10.1126/sciadv.1601278

Pearson, D. G., Brenker, F. E., Nestola, F., McNeill, J., Nasdala, L., Hutchison, M. T., et al. (2014). Hydrous mantle transition zone indicated by ringwoodite included within diamond. *Nature*, *507*(7491), 221–224. https://doi.org/10.1038/nature13080

Perdew, J. P., Burke, K., & Ernzerhof, M. (1996). Generalized gradient approximation made simple. *Physical Review Letters*, *77*(18), 3865–3868. https://doi.org/10.1103/PhysRevLett.77.3865

Poe, B. T., Romano, C., Liebske, C., Rubie, D. C., Terasaki, H., Suzuki, A., & Funakoshi, K. (2006). High-temperature viscosity measurements of hydrous albite liquid using in-situ falling-sphere viscometry at 2.5 GPa. *Chemical Geology*, *229*(1–3), 2–9. https://doi.org/10.1016/j.chemgeo.2006.01.010

Pöhlmann, M., Benoit, M., & Kob, W. (2004). First-principles molecular-dynamics simulations of a hydrous silica melt: Structural properties and hydrogen diffusion mechanism. *Physical Review B*, *70*(18), 184209. https://doi.org/10.1103/PhysRevB.70.184209

Pommier, A., Gaillard, F., Pichavant, M., & Scaillet, B. (2008). Laboratory measurements of electrical conductivities of hydrous and dry Mount Vesuvius melts under pressure. *Journal of Geophysical Research*, *113*, B05205. https://doi.org/10.1029/2007jb005269

Posner, E. S., Steinle-Neumann, G., Vlček, V., & Rubie, D. C. (2017). Structural changes and anomalous self-diffusion of oxygen in liquid iron at high pressure. *Geophysical Research Letters*, *44*, 3526–3534. https://doi.org/10.1002/2017GL072926

Revenaugh, J., & Sipkin, S. A. (1994). Seismic evidence for silicate melt atop the 410-km mantle discontinuity. *Nature*, *369*(6480), 474–476. https://doi.org/10.1038/369474a0

Richet, P., Whittington, A., Holtz, F., Behrens, H., Ohlhorst, S., & Wilke, M. (2000). Water and the density of silicate glasses. *Contributions to Mineralogy and Petrology*, *138*(4), 337–347. https://doi.org/10.1007/s004100050567

Sakamaki, T., Ohtani, E., Urakawa, S., Suzuki, A., & Katayama, Y. (2009). Measurement of hydrous peridotite magma density at high pressure using the X-ray absorption method. *Earth and Planetary Science Letters*, *287*(3–4), 293–297. https://doi.org/10.1016/j.epsl.2009.07.030

Sakamaki, T., Suzuki, A., & Ohtani, E. (2006). Stability of hydrous melt at the base of the Earth's upper mantle. *Nature*, *439*(7073), 192–194. https://doi.org/10.1038/nature04352

Schmandt, B., Jacobsen, S. D., Becker, T. W., Liu, Z., & Dueker, K. G. (2014). Dehydration melting at the top of the lower mantle. *Science*, *344*(6189), 1265–1268. https://doi.org/10.1126/science.1253358

Schwegler, E., Sharma, M., Gygi, F., & Galli, G. (2008). Melting of ice under pressure. *Proceedings of the National Academy of Sciences of the United States of America*, *105*(39), 14,779–14,783. https://doi.org/10.1073/pnas.0808137105

Spiekermann, G., Wilke, M., & Jahn, S. (2016). Structural and dynamical properties of supercritical H_2O-SiO_2 fluids studied by ab initio molecular dynamics. *Chemical Geology*, *426*, 85–94. https://doi.org/10.1016/j.chemgeo.2016.01.010

Stixrude, L., & Karki, B. (2005). Structure and freezing of $MgSiO_3$ liquid in Earth's lower mantle. *Science*, *310*(5746), 297–299. https://doi.org/10.1126/science.1116952

Stolper, E. (1982). The speciation of water in silicate melts. *Geochimica et Cosmochimica Acta*, *46*(12), 2609–2620. https://doi.org/10.1016/0016-7037(82)90381-7

Takahashi, E. (1986). Melting of a dry peridotite KLB-1 up to 14 GPa: Implications on the origin of peridotitic upper mantle. *Journal of Geophysical Research*, *91*(B9), 9367–9382. https://doi.org/10.1029/JB091iB09p09367

Tauzin, B., Debayle, E., & Wittlinger, G. (2010). Seismic evidence for a global low-velocity layer within the Earth's upper mantle. *Nature Geoscience*, *3*(10), 718–721. https://doi.org/10.1038/ngeo969

Thomas, C. W., & Asimow, P. D. (2013). Preheated shock experiments in the molten $CaAl_2Si_2O_8$-$CaFeSi_2O_6$-$CaMgSi_2O_6$ ternary: A test for linear mixing of liquid volumes at high pressure and temperature. *Journal of Geophysics Research: Solid Earth*, *118*, 3354–3365. https://doi.org/10.1002/jgrb.50269

Tian, Y., Zhu, H., Zhao, D., Liu, C., Feng, X., Liu, T., & Ma, J. (2016). Mantle transition zone structure beneath the Changbai volcano: Insight into deep slab dehydration and hot upwelling near the 410 km discontinuity. *Journal of Geophysical Research: Solid Earth*, *121*, 5794–5808. https://doi.org/10.1002/2016JB012959

Toffelmier, D. A., & Tyburczy, J. A. (2007). Electromagnetic detection of a 410-km-deep melt layer in the southwestern United States. *Nature*, *447*(7147), 991–994. https://doi.org/10.1038/nature05922

Tschauner, O., Huang, S., Greenberg, E., Prakapenka, V. B., Ma, C., Rossman, G. R., et al. (2018). Ice-VII inclusions in diamonds: Evidence for aqueous fluid in Earth's deep mantle. *Science*, *359*(6380), 1136–1139. https://doi.org/10.1126/science.aao3030

Winkler, A., Horbach, J., Kob, W., & Binder, K. (2004). Structure and diffusion in amorphous aluminum silicate: A molecular dynamics computer simulation. *The Journal of Chemical Physics*, *120*(1), 384–393. https://doi.org/10.1063/1.1630562

Wirth, R., Vollmer, C., Brenker, F., Matsyuk, S., & Kaminsky, F. (2007). Inclusions of nanocrystalline hydrous aluminium silicate "Phase Egg" in superdeep diamonds from Juina (Mato Grosso State, Brazil). *Earth and Planetary Science Letters*, *259*(3–4), 384–399. https://doi.org/10.1016/j.epsl.2007.04.041

Xia, Q.-K., Bi, Y., Li, P., Tian, W., Wei, X., & Chen, H. L. (2016). High water content in primitive continental flood basalts. *Scientific Reports*, *6*(1), 25,416. https://doi.org/10.1038/srep25416

Xin, J., Gan, L., Wang, N., & Chen, M. (2019). Accurate density calculation for molten slags in SiO_2-Al_2O_3-CaO-MgO-'FeO'-'Fe_2O_3' systems. *Metallurgical and Materials Transactions B: Process Metallurgy and Materials Processing Science*, *50*(6), 2828–2842. https://doi.org/10.1007/s11663-019-01674-1

Xue, X., & Kanzaki, M. (2004). Dissolution mechanisms of water in depolymerized silicate melts: Constraints from ^{1}H and ^{29}Si NMR spectroscopy and ab initio calculations. *Geochimica et Cosmochimica Acta*, *68*(24), 5027–5057. https://doi.org/10.1016/j.gca.2004.08.016

Yamada, A., Inoue, T., Urakawa, S., Funakoshi, K. I., Funamori, N., Kikegawa, T., & Irifune, T. (2011). In situ X-ray diffraction study on pressure-induced structural changes in hydrous forsterite and enstatite melts. *Earth and Planetary Science Letters*, *308*(1–2), 115–123. https://doi.org/10.1016/j.epsl.2011.05.036

Yamada, A., Inoue, T., Urakawa, S., Funakoshi, K. I., Funamori, N., Kikegawa, T., et al. (2007). In situ X-ray experiment on the structure of hydrous Mg-silicate melt under high pressure and high temperature. *Geophysical Research Letters*, *34*, L10303. https://doi.org/10.1029/2006GL028823

Yuan, L., & Steinle-Neumann, G. (2020). Strong sequestration of hydrogen into the Earth's core during planetary differentiation. *Geophysical Research Letters*, *47*, e2020GL088303. https://doi.org/10.1029/2020gl088303

Zhang, J., & Herzberg, C. (1994). Melting experiments on anhydrous peridotite KLB-1 from 5.0 to 22.5 GPa. *Journal of Geophysical Research*, *99*, 17,729–17,742. https://doi.org/10.1029/94jb01406

Zhang, Y., Wang, C., Jin, Z., & Zhu, L. (2017). Partial melting of stagnant oceanic lithosphere in the mantle transition zone and its geophysical implications. *Lithos*, *292–293*, 379–387. https://doi.org/10.1016/j.lithos.2017.09.019

Zhao, D., Tian, Y., Lei, J., Liu, L., & Zheng, S. (2009). Seismic image and origin of the Changbai intraplate volcano in East Asia: Role of big mantle wedge above the stagnant Pacific slab. *Physics of the Earth and Planetary Interiors*, *173*(3–4), 197–206. https://doi.org/10.1016/j.pepi.2008.11.009

Zotov, N., Keppler, H., Hannon, A. C., & Soper, A. K. (1996). The effect of water on the structure of silicate glasses—A neutron diffraction study. *Journal of Non-Crystalline Solids*, *202*(1–2), 153–163. https://doi.org/10.1016/0022-3093(96)00149-4

Zotov, N., Yanev, Y., Epelbaum, M., & Konstantinov, L. (1992). Effect of water on the structure of rhyolite glasses—X-ray diffraction and Raman spectroscopy studies. *Journal of Non-Crystalline Solids*, *142*, 234–246. https://doi.org/10.1016/S0022-3093(05)80030-4